Nakato *et al. Earth, Planets and Space (2023) 75:45*
https://doi.org/10.1186/s40623-022-01754-8

Earth, Planets and Space

FRONTIER LETTER

Open Access

Variations of the surface characteristics of Ryugu returned samples

Aiko Nakato[1*], Toru Yada[1], Masahiro Nishimura[1], Kasumi Yogata[1], Akiko Miyazaki[1], Kana Nagashima[1], Kentaro Hatakeda[1,7], Kazuya Kumagai[1,7], Yuya Hitomi[1,7], Hiromichi Soejima[1,7], Jean-Pierre Bibring[2], Cedric Pilorget[2], Vincent Hamm[2], Rosario Brunetto[2], Lucie Riu[3], Lionel Lourit[2], Damien Loizeau[2], Tania Le Pivert-Jolivet[2], Guillaume Lequertier[2], Aurelie Moussi-Soffys[4], Masanao Abe[1,8], Tatsuaki Okada[1], Tomohiro Usui[1], Satoru Nakazawa[1], Takanao Saiki[1], Satoshi Tanaka[1], Fuyuto Terui[5], Makoto Yoshikawa[1], Sei-ichiro Watanabe[6] and Yuichi Tsuda[1,8]

Abstract

Hayabusa2 spacecraft successfully collected rock samples from the surface of C-type near-Earth asteroid 162173 Ryugu through two touchdowns and brought them back to Earth in 2020. At the Extraterrestrial Sample Curation Center in JAXA, we performed initial description of all samples to obtain fundamental information and prepare the database for sample allocation. We propose morphological classifications for the returned samples based on the initial description of 205 grains described in the first 6 months. The returned samples can be distinguished by four morphological characteristics: dark, glossy, bright, and white. According to coordinated study to provide an initial description and detailed investigation by scanning electron microscopy and X-ray diffraction analysis in this study, these features reflect the differences in the degree of space weathering and mineral assemblages. The degree of space weathering of the four studied grain types is heterogeneous: weak for A0042 (dark group) and C0041 (white group); moderate for C0094 (glossy); and severe for A0017 (bright). The white phase, which is the mineral characteristic of the white group grains, is identified as large carbonate minerals. This is the first effort to classify Ryugu returned samples into distinct categories. Based on these results, researchers can estimate sample characteristics only from the information on the JAXA curation public database. It will be an important reference for sample selection for further investigation.

Keywords Hayabusa2, Ryugu, Curation, Returned samples, Classification

*Correspondence:
Aiko Nakato
nkt.aiko@gmail.com
Full list of author information is available at the end of the article

Graphical Abstract

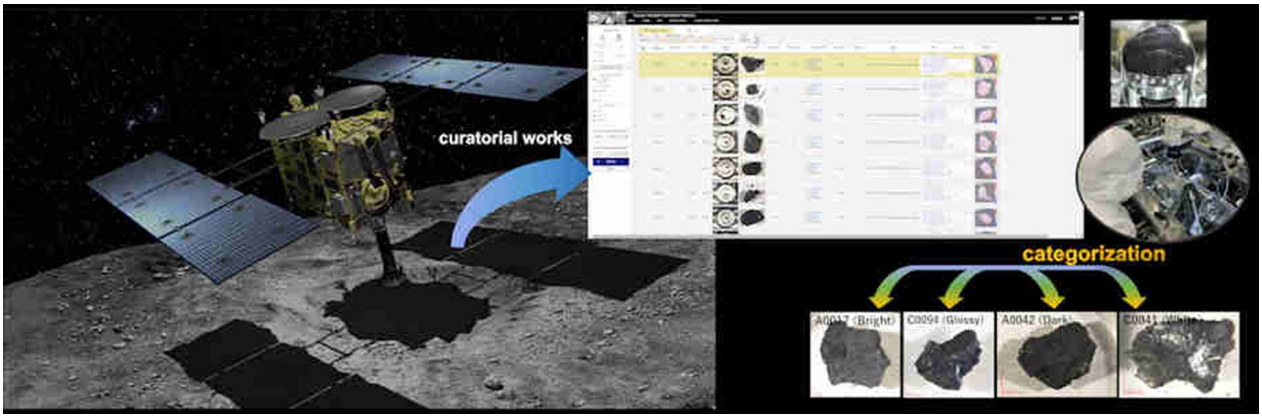

Introduction

On December 6, 2020, the Hayabusa2 spacecraft successfully returned samples from the C-type asteroid 162173 Ryugu to Earth (Tsuda et al. 2020). Upon return, the sample catcher that collected the samples was installed in a clean chamber in the Extraterrestrial Sample Curation Center (ESCuC) at Sagamihara campus, Institute of Space and Astronautical Science (ISAS), Japan, under vacuum conditions (Tachibana et al. 2022). The Clean Chambers (CCs) consist of five rooms, with two rooms CC3-1 and -2 that are held at a vacuum, two rooms CC4-1 and -2, where pure nitrogen circulates, and one room CC3-3 that acts as an airlock between CC3-2 and CC4-1. Two sample grains, several microns in size, have been removed from the sample catcher and stored in a vacuum environment in CC3-2 for future research. All the remaining samples have been placed in a pure nitrogen environment and are handled only through gloves (Yada et al. 2022). For curation, initial descriptions, photography and weight measurements of the samples have been carried out. Based on the design weight of the catcher and pre-measured weight of the handling jig constructed to handle the catcher, the calculated total weight of samples inside the catcher is 5.424 ± 0.217 g (Yada et al. 2022). The samples have been moved from each chamber of the catcher to small containers called the "bulk dishes", which are made of sapphire glass each with a diameter of 23 mm. Samples in the bulk dishes were initially described with non-destructive techniques by microscopy, weighing, Fourier transform Infrared Spectroscopy (FT-IR) (Yada et al. 2022; Miyazaki et al., in preparation; Hatakeda et al. 2023), and MicrOmega hyperspectral imaging (Pilorget et al. 2021a, b; Yogata et al., in preparation).

By the end of June 2021, as part of the curatorial work, a total of 205 sample grains have been picked from the bulk dishes, which comprise 100 grains from chamber A of the sample catcher taken at the first touchdown site (TD1) and 105 grains from chamber C taken at the second touchdown site (TD2) near the artificial crater formed by the small carry-on impactor (SCI) (Arakawa et al. 2020). It is about one quarter of the returned sample weight. To obtain the size distribution of returned samples as soon as possible, we picked up the grains in order from the largest one. The sample grains were individually moved to a smaller dish, 15 mm in diameter and 3 mm in depth, made of sapphire using vacuum tweezers, and each dish was covered with a quartz window and then stored in CC4-1 under a pure nitrogen environment. Each sample collected from sample container A during TD1 was named 'Sample A', and each sample collected into sample chamber C during TD2 was named 'Sample C'. During the initial description of the individual grains, the quartz window was temporarily removed, and the workflow was applied in the same manner as for the non-destructive bulk descriptions by microscopy, weighing, FT-IR and MicrOmega hyperspectral imaging. The information obtained through these initial descriptions is registered in the curation database (https://darts.isas.jaxa.jp/curation/hayabusa2/). Researchers can access the database worldwide and select samples for the International Announcement Opportunity (Int'l AO) of Ryugu samples.

In this study, taking advantage of the uniqueness of the JAXA curatorial work that has handled large numbers of samples, we propose four morphological classifications (dark, glossy, bright, and white) for the 205 grains

registered in the database, based on optical microscopic observations. Details of each morphological classification will be described in the next section (Sample Categorization). Four grains representing each of the four groups were delineated as JAXA detailed description (JAXA-DD) samples. The JAXA-DD is a detailed characterization including some destructive analytical methods performed inside ESCuC on some individual particles as a part of the JAXA initial description. The purpose of this paper is to provide information that can be used as a reference for sample distribution to various stakeholder groups, including: the nominated initial analysis team, Phase 2 curation team which is detailed curation with collaborating institutes, NASA for sample exchange between Hayabusa2 and OSIRIS-REx missions according to JAXA-NASA mutual agreement, and sample selection for the Int'l AO. The sample distribution and the proportion were approved by the Hayabusa2 Sample Allocation Committee, which consists of researchers from throughout the world. For the JAXA-DD, up to 2 wt. % of the returned samples can be distributed, and the four particles allocated in this study account for ~ 0.5 wt. %. This is the first attempt to link the morphological appearance of the grains with their mineralogy, petrology, and spectral features, based on the detailed information obtained in this study and the information registered in the database collected during the JAXA initial descriptions of the Ryugu samples. Our study will guide future researchers when selecting grains from the curation database catalog for analysis. In addition, by linking the detailed analytical results of the initial analysis teams and Phase 2 teams, it is expected that information regarding the grain surface and interior can be correlated, which will provide further insights into the nature and evolution of asteroid Ryugu.

Samples and experiments

Sample categorization

Based on the images obtained by optical microscopy in the JAXA initial descriptions, the proposed morphological classification is described below (Fig. 1). In the initial

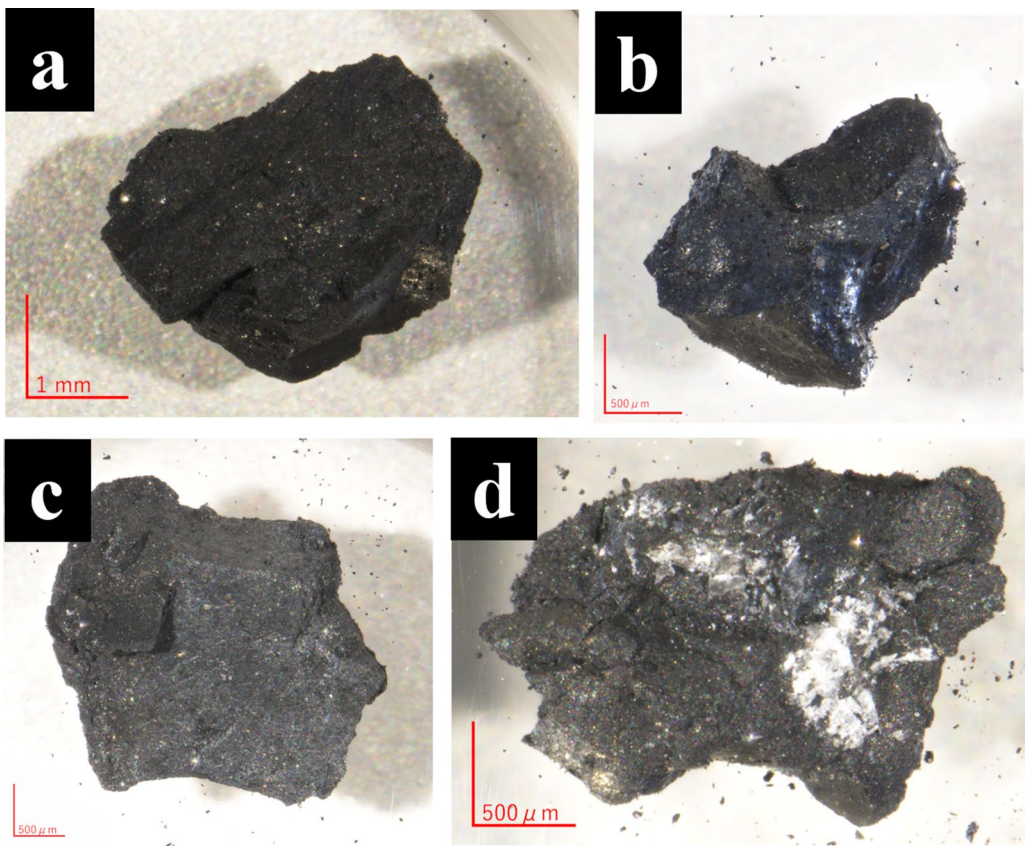

Fig. 1 Microscopic images of four representative grains. **a** A0042, dark group. This feature is dominant in Ryugu returned samples. **b** C0094, glossy group. Especially, the bottom part of this image shows shiny and glossy reflection. **c** A0017, bright group. Most of the flat surface of this grain shows bright color excluding upper left region corresponding with the dark lithology. **d** C0041, white group. One-third of this grain exhibits white inclusions

description, only one side of each grain was described due to time constraints. Therefore, the morphological classification proposed in this study is based on the optical microscopy images of one side of each grain that were archived in the database.

(1) Dark group: The typical, dark-colored grains of the Ryugu returned samples. Many of these grains have large uneven morphologies on the scale of 0.5 to several mm and are also covered with fine particles on their surfaces.
(2) Glossy group: More than one-third of the entire surface of each of these grains are smooth and have a specular luster.
(3) Bright group: More than one-third of the entire surface of each of these grains has a light gray appearance as compared with the other grains. These grains do not have a smooth structure like those of the glossy group, and do not exhibit large uneven morphology or have fine particles covering grain surfaces, like those of the dark group.
(4) White group: Each of these grains contains white materials of >300 μm^2 in size on their surfaces of the grains.

Each abundance is given in percentage. The total abundance exceeds 100%, because two or more group characteristics apply to a single grain.

Table 1 shows the abundance of grains in each group. The classification table for all grains is summarized in Additional file 1 Material. Grains of all four groups are found in both the TD1 and TD2 samples. In some cases, two or more group characteristics apply to a single grain, and thus, the total abundance exceeds 100%. Due to the high abundance of grains of dark group, over 70% of the other three characteristics occur together with dark morphology. As second most accompanying characteristic, the bright and glossy groups share several tens of percent of the characteristics with each other. Approximately 95% of the 205 grains belong to the dark group, indicating that the returned samples are dominated by very low reflectance materials (Table 1). These observations are consistent with results of bulk sample examined by FTIR and MicrOmega (Yada et al. 2022). The abundances of grains with the characteristics of the white and bright groups are 5.9% and 12.7%, respectively, indicating that ~ 10% of the returned samples are bright materials. Miyazaki et al., (in preparation) observed more than 600 returned samples and reported that the abundance of grains corresponding to the white group is ~ 5%, which is similar to that of this study. There is little difference between the TD1 and TD2 samples in terms of the abundances of grains in Dark, Glossy and White groups. However, grains classified as being in the bright group in the TD1 samples, taken from the surface layer, are approximately 1.7 times as abundant as those in the TD2 samples, which are thought to contain subsurface materials. Based on the detailed analysis described in the discussion section, this difference may reflect the degree of space weathering at the sampling locations.

The surface materials of Ryugu are considered to be a mixture of multiple types of grains as represented by the returned samples. The albedo of the asteroid Ryugu was obtained from remote sensing observations by the Telescopic Optical Navigation Camera (ONC-T) is ~ 2% (Pilorget et al. 2021a, b), and it is the lowest reflectance object ever observed (Tatsumi et al. 2020). The observational results of the Mobile Asteroid Surface Scout Camera (MASCOT/CAM) lander onboard the Hayabusa2 spacecraft identified about 10 vol. % "bright" materials (Jaumann et al. 2019). Spectrally, the bright materials have some variation based on the colors, which can be distinguished by the blue and red, at least. The average size of these bright inclusions is 0.38 ± 0.55 mm (Jaumann et al. 2019), which is consistent with the size range of the returned samples. The observation results of MASCOT/CAM and the optical characteristics of the 205 returned samples are generally consistent. The colors of inclusions reflect the compositional differences. The MASCOT/CAM has not yet identified the nature/composition of the bright materials because of the lack of

Table 1 Classification of 205 grains based on their morphology

Characteristic	# of TD1 grain	Abundance in 100 TD1 grains	# of TD2 grain	Abundance in 105 TD2 grains	Abundance in 205 grains	Most accompanying characteristic and the abundance	Second most accompanying characteristic and the abundance
Dark	94	94.0	102	97.1	95.6	Glossy-16	Bright-10
Glossy	16	16.0	19	18.1	17.1	Dark-91	Bright-23
Bright	16	16.0	10	9.5	12.7	Dark-73	Glossy-31
White	6	6.0	6	5.7	5.9	Dark-83	Glossy and Bright-17

spectral data > 1 μm in wavelength, but the JAXA-DD and further investigations of the returned samples may reveal their nature. Previous studies in which the TD1 and TD2 samples were investigated as aggregate "bulk" samples reported that the Hayabusa2 returned samples have characteristics representative of typical boulders on the surface of Ryugu in terms of spectral features (Pilorget et al. 2021a, b; Yada et al. 2022). In this study, we classified 205 grains individually taken from the bulk samples, based on optical characteristics, and also confirmed that the returned samples are representative of the surface of Ryugu.

Samples and methods

We selected one representative grain from each group: A0042 that has a dark appearance typical of Ryugu samples; C0094 that has glossy characteristics; A0017 that is mostly bright; and C0041 that is covered by ~ 30% of white material on the front surface of the grain (Fig. 1). Feret diameters and weights of each grain are as follows: A0042 = 3.784 mm and 11.9 mg; C0094 = 2.181 mm and 3.1 mg; A0017 = 3.748 mm and 8.3 mg; C0041 = 2.615 mm and 3.3 mg. The maximum Feret diameter (i.e., the caliper diameter) was measured using the imaging software ImageJ, and is registered in the database as the particle size.

Figure 2 shows a flow chart of the analytical protocols of the allocated JAXA-DD grains. In the normal workflow of the JAXA initial descriptions, only one side of the grains was observed and photographed by optical microscopy, but for the four grains in this study, the back surfaces of the grains were subsequently photographed in CC4-2. For the microscope, we have developed an electric control stage based on the Nikon SMZ1270i binocular stereomicroscope. Using the electric control stage, a high magnification map and omni focal image of each grain was taken. We tried to measure accurate dimensions by scale calibration each time the magnification was changed. Flexible arm LED light lamp was used to illuminate each grain in two directions. The brightness was adjusted, so that the grain shadows were even and the illumination was the same for each grain.

Approximately one-third of the back side of A0017 has a bright area similar to the front side of the grain. The back side of C0094 has glossy characteristics like the front side. In contrast, the back surfaces of C0041 and A0042 have the same dark appearance as the front surface of A0042, which is typical of Ryugu returned samples.

The four grains were sealed one by one in a transport container called the Facility to Facility Transfer Container (FFTC) developed by the Phase 2 curation Kochi team (Ito et al. 2020) in CC4-1. These were then transferred to a pure nitrogen environment glove box (GB1) constructed with stainless steel and with a glass window. In GB1, the grains were transferred to a sealed Field

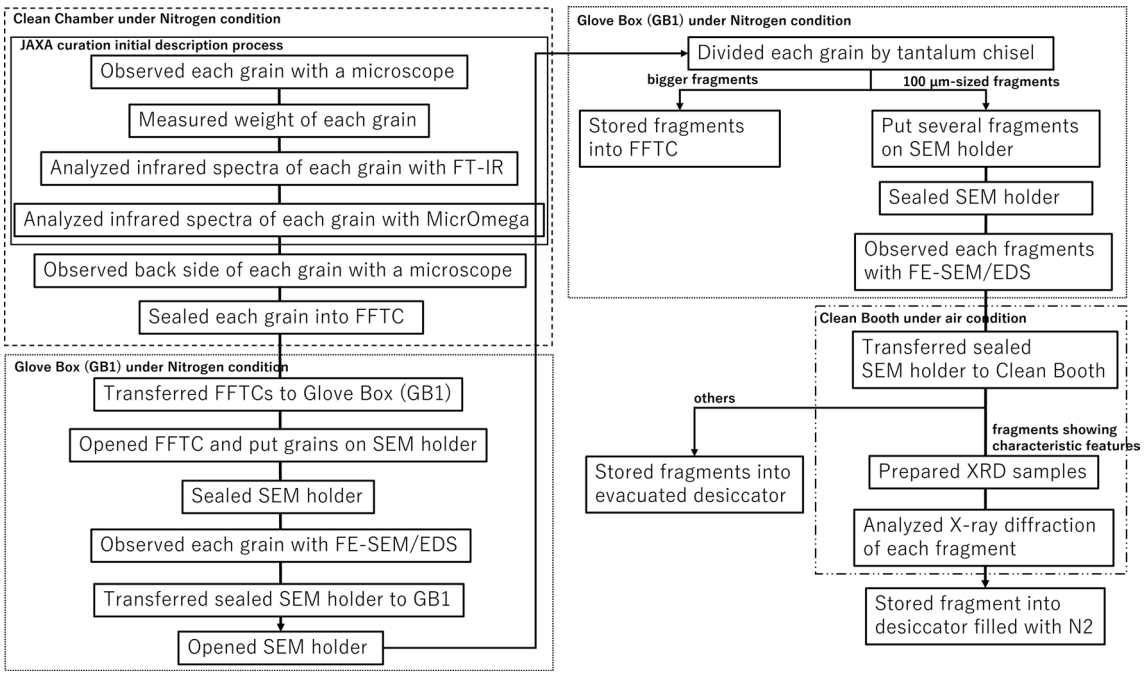

Fig. 2 Flowchart of a series of processes for JAXA-DD samples. Note that the majority of grains have only been exposed to vacuum and nitrogen environment in clean chamber and glove box, and then have been stored under nitrogen environment

Emission–Scanning Electron Microscopy (FE–SEM) holder made of aluminum, and the SEM holder was loaded into a Hitachi SU6600 FE–SEM–EDS (Energy Dispersive X-ray Spectroscopy). The SEM is equipped with an Oxford X-Max 150 EDS detector, which is 150 mm^2 silicon drift detector. High-resolution observations and chemical analyses of the grain surfaces were carried out without coating, fixation, or air exposure. For the microstructural observations, a low-vacuum mode (~ 60 Pa), and accelerating voltage of 15 kV, and a measured beam current of ~ 0.3 nA were used to avoid charging and drift of the non-coated sample. The EDS analysis was undertaken in high-vacuum mode ($\leq 1 \times 10^{-3}$ Pa), with an accelerating voltage of 15 kV and a measured beam current of ~ 0.25 nA, to prevent scattering of the irradiated electrons.

Based on the mineralogical and petrological information obtained by FE–SEM–EDS, each grain was divided using a tantalum chisel in GB1. The sample division method using this chisel has been improved for smaller samples based on the method of the Antarctic Meteorite Research Center, National Institute of Polar Research (Yamaguchi 2020). We designed and manufactured a positioning jig with Narishige Kagaku Kikai Kenkyusho Company that can divide the target area in a small grain inside the glovebox, which only uses limited materials to prevent sample contamination (Fig. 3). For the chisel material, tantalum was selected due to its hardness and to reduce possible contamination, as it was also used for the sampling projectiles on Ryugu (Sawada et al. 2017). The cutting edge of the chisel is 1 mm wide, and the tip was polished by hand using a diamond grindstone.

The larger sub-grains were moved to a single sapphire dish, sealed in FFTC, and stored in a nitrogen environment. The smaller sub-grains with sizes of 100–200 μm were placed on a sealed FE–SEM holder. FE–SEM–EDS observations of the samples were re-performed without exposure to air in the same manner as before the grains were divided. After the SEM observations, four to five fragments with representative characteristics were selected for each group and used for X-ray diffraction (XRD) analysis. These samples were fixed to the tip of a 5 μm diameter carbon fiber with crystal bond, and analyzed with a Rigaku RA-Micro7 HFMR XRD instrument

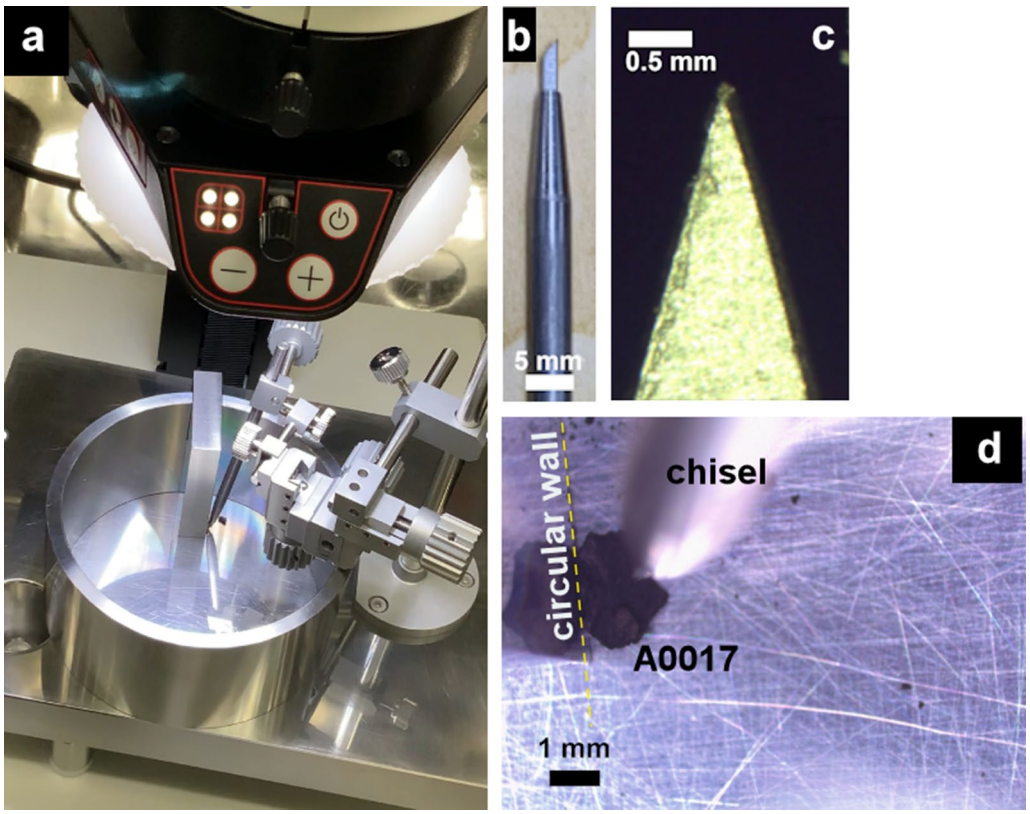

Fig. 3 Chisel setup for the sample division. **a** Chisel setup under microscope in the glovebox. A circular wall is used to fix the sample and prevent from scattering of divided samples. **b** Photo of a tantalum chisel. **c** Photo of the cutting edge of a tantalum chisel after polished by hand using a diamond grindstone. **d** Microscopic image of sample division. This image was taken just before the division of A0017. The grain was fixed between the circular wall and the chisel

using a copper target. The acquired XRD patterns were analyzed with the Rigaku PDXL software. The above 4 to 5 smaller fragments that were specifically selected for XRD analysis were exposed to Earth's atmosphere. However, most of the samples, excluding dozens of 100 micron or less sized fragments, for XRD were only handled in a pure nitrogen environment throughout all the analytical steps and are still stored in the same environment for future analysis.

Results

Petrology and chemistry

The petrology and chemical composition of the matrix of each group obtained by FE–SEM–EDS observations are as follows.

Dark group (A0042)

The main minerals are hexagonal platy pyrrhotite, carbonate, magnetite with four morphologies (framboidal, plaquette, spherulitic, and cubic), and coarse-grained phyllosilicate (Fig. 4a–e). These minerals are embedded in a fine-grained phyllosilicate-rich matrix. Euhedral pyrrhotite is predominant and occurs as single crystals larger than 0.5 μm. The pyrrhotite has smooth and stepped grain surfaces, which may reflect crystal growth or dissolution in aqueous solutions. Carbonate with a diameter of 5–30 μm is also ubiquitous in the matrix. Given the small grain size and slanted surface of A0042, it was difficult to quantitatively analyze the chemical composition of the carbonate in the high-vacuum mode due to charge-up. However, semi-quantification in the low-vacuum mode confirmed that the composition is similar to an Mg–Ca carbonate (i.e., a dolomite compositional range). In addition, numerous circular structures with a maximum diameter of ~ 1 μm are scattered in the matrix (Fig. 4f, g).

Glossy group (C0094)

Like A0042, this sample contains hexagonal platy pyrrhotite, carbonate, magnetite with four morphologies (framboidal, plaquette, spherulitic, and cubic), and coarse-grained phyllosilicate (Fig. 5a–f). Pyrrhotite has smooth and stepped surfaces like A0042, and some grains throughout the matrix have burst vesicle-like textures (Thompson et al. 2019; 2020) on their surface. Although the carbonate is also small, with diameters of 5–20 μm, quantitative EDS analysis could be performed because of the smooth and flat surface of C0094 and yielded a dolomite composition (Fig. 6). In C0094, melt-like droplets that are ~ 5 μm in size were observed in the matrix (Fig. 5i). The melt droplets are rounded in shape and contain spherical inclusions of opaque minerals. The chemical composition of each melt droplet is different, with some being depleted in light elements and others having the same composition as the surrounding matrix. In addition, some melt droplets have a melt aggregate structure (Fig. 5j). In the region, where the melt droplets are abundant, a particularly large number of dark circular structures are evident in back-scattered electron (BSE) images (Fig. 5g, h). EDS line analysis of the circular structures did not identify increased concentrations of specific elements, such as organic matter, in the structure interiors, and the rim has elemental concentrations similar to the surrounding matrix. As such, the circular structures are presumed to be concave holes similar to a crater and/or burst vesicle (Fig. 5k). Compared to the circular structures in A0042, those in C0094 are larger and have a clear boundary with the matrix due to the surrounding rims.

Bright group (A0017)

Approximately 80% of the front surface of this grain is bright, and the remaining 20% is dark (Fig. 1c). On the back side of the grain, at least 30% is bright. There is no significant difference between the mineralogy of the two lithologies. Hexagonal platy pyrrhotite, carbonate, magnetite with three morphologies (framboidal, plaquette, and spherulitic), and coarse-grained phyllosilicate are found in both lithologies (Fig. 7a–f). Unlike A0042 and C0094, A0017 contains relatively large dolomite grains with diameters of 40–100 μm in both lithologies (Fig. 7e). Pyrrhotite with the altered surface texture that occurred in C0094 was observed in the bright lithology of A0017. On the front surface of A0017, altered and smooth pyrrhotite coexist in the bright lithology and, on the back side of the grain, only altered pyrrhotite occurs (Fig. 7a, b). In contrast, where dark lithologies characterize both surfaces, only smooth pyrrhotite is present and no altered pyrrhotite is visible. Textures such as melt droplets and the circular structures were only observed in the bright lithology (Fig. 7g–i). Numerous circular structures have rims, and the boundaries with the matrix are clearer than those of C0094. Similar to C0094, the composition of each melt droplet is variable. Near the region of abundant melt droplets, a bleb-rich, melt vein-like texture (Fig. 7j) and a melt aggregate texture occur over an area of ~ 200 μm^2 (Fig. 7k, l).

White group (C0041)

Approximately 30% of the front surface is covered with white materials, which are visible under an optical microscope. Based on the FE–SEM–EDS results, this grain consists mainly of hexagonal platy pyrrhotite, carbonate, magnetite with three morphologies (framboidal, plaquette, and spherulitic), and coarse-grained phyllosilicate (Fig. 8a–e). The Mg–Ca carbonate minerals found in the other three groups of grains were rarely identified by FE–SEM–EDS observations. Although there is a carbonate having

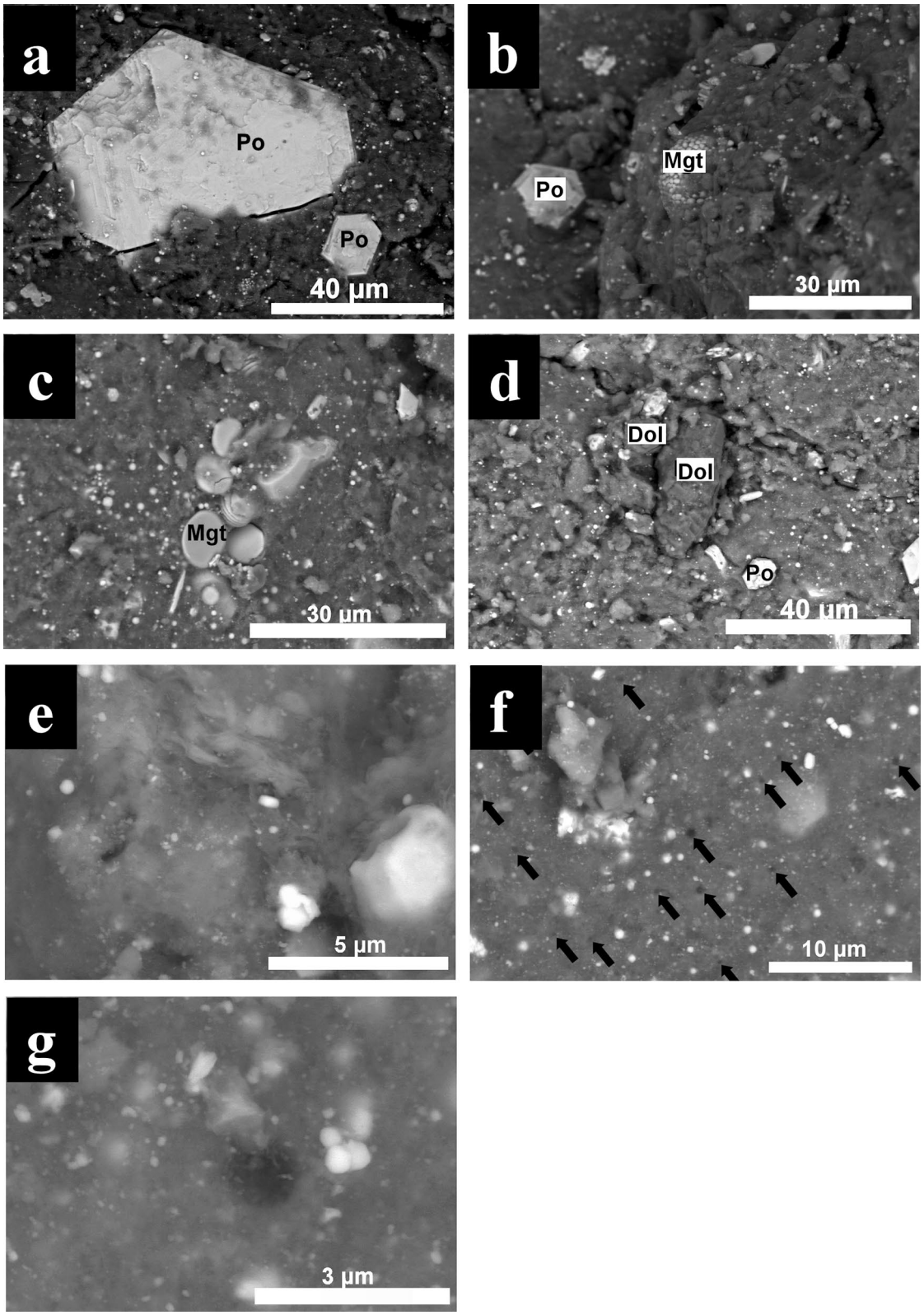

Fig. 4 Back-scattered electron images of major constituent phases in A0042, dark group. **a** Euhedral hexagonal morphology of pyrrhotite showing a smooth texture. **b** Framboidal magnetite. **c** Plaquette magnetite. **d** Ca–Mg carbonate, dolomite. **e**) Coarse-grained phyllosilicate. **f** Circular structure-enriched region. Larger ones are indicated by arrows. **g** High-resolution image of a circular structure

dolomite-like composition, it is difficult to analyze quantitively because of the tiny size, submicron in width and less than 10 microns in length, and the markedly uneven location between framboidal magnetite grains. Since the samples are non-coated and non-fixed, smaller minerals move easily by charging and were not able to be analyzed by EDS. Instead, large Mg–Fe carbonate minerals with diameters of > 100 μm occur locally in C0041, and some single crystals appear to have grid-like cracks (Fig. 8d). These Mg–Fe carbonate minerals coincide with the areas that appear white under the microscope. Although there are sub-micron-sized circular structures (Fig. 8f, g), no rims surround the circular structures, and melt droplets are absent.

To determine the chemical composition of the matrix, several tens of EDS analyses were carried out on each sample, which avoided the large opaque minerals (Fig. 6a). Most data have (Si + Al):Mg:Fe of 4–6:3–5:0.5–2.0. These data suggest that the main minerals in the matrix are a mixture of serpentine and saponite in various proportions. Data for the four groups of grains overlap, but several analyses of A0017 are more Fe-rich. The compositional data for the bright and dark lithologies in A0017 show that the bright lithology has a large variation in Fe content, and that the dark lithology is similar to the other three groups (Fig. 6b).

The carbonate minerals have dolomite composition, except in C0041 (Fig. 6c). The Mg–Fe carbonate mineral in C0041 has a wide range of compositions, which are between siderite–magnesite (or breunnerite), and have Fe concentrations of 2–55 wt. %.

Mineral assemblages

Figure 9 shows XRD patterns of each morphological group. Each pattern in Fig. 9 was selected from the perspective that the most minerals are detected in a fragment. The minerals identified by XRD in all four groups are serpentine, saponite, magnetite, pyrrhotite, dolomite, and pentlandite. In all groups, the 0.73 nm reflection of serpentine and prism reflections of saponite and serpentine were detected. These mineral assemblages are consistent with those inferred from SEM–EDS observations. In the 100-μm-sized sub-samples, dolomite was either detected or not detected. Therefore, A0017 in Fig. 9 does not show dolomite peak in the pattern. Dolomite in C0041 was not detected by SEM–EDS, but was detected by XRD when we avoided the large white region and selected matrix fragment. These results show that the dolomite is heterogeneously distributed on a 100 μm scale. The mineral corresponding to the white region of C0041 is classified as Fe-rich magnesite (or breunnerite), based on the chemical composition obtained by SEM–EDS, but siderite was identified by XRD. This siderite was not detected in the other groups of grains by either XRD or SEM–EDS.

Discussion

Weathering of sample surfaces on the asteroid

Based on the petrological observations, chemical compositions of the matrix, and mineral assemblages, the four grains are similar to CI chondrites, although there are variations in appearance, as documented in previous studies (Nakamura et al. 2022; Noguchi et al. 2022; Yokoyama et al. 2022). Given that sulfate and ferrihydrite, which typically occur in CI chondrites, are not observed in the Ryugu samples, previous studies have suggested that these minerals may be the result of terrestrial alteration of CI chondrites (Noguchi et al. 2022; Yabuta et al., submitted to Science). Ferrihydrite is difficult to detect with our analytical methods, but sulfate was also not found by the JAXA-DD. Sulfate is absent in the SEM observations carried out without exposure to air, and also absent in the XRD analysis, where small rock fragments were exposed to the atmosphere. Sulfate was probably not produced even in the air-exposed samples, due to relatively a short period of time from division of the samples to XRD analysis in a week, and due to conditioned low humidity in the room.

All four grains contain the circular structures and range in size up to a few microns in diameter in the phyllosilicate matrices. The structure is very similar to crater and/or burst vesicle. Some of them show clear rims with crater morphology as reported in Itokawa particles (Matsumoto et al. 2018). On the other hand, the observation that the circular structures look empty is similar to burst vesicles (Thompson et al. 2019; 2020). The burst vesicles might be produced by degassing of structural water from amorphous phyllosilicate. The degree of amorphization of phyllosilicate increases with progressive laser irradiation (Thompson et al. 2020). Either way, presence of the circular structures suggests that the grain surface experienced space weathering by micrometeoroid impact.

Unlike meteorite samples that largely originate from the interiors of parent bodies, all four of the studied Ryugu grains are likely to have undergone space weathering processes on the surface of Ryugu based on the presence of craters and/or burst vesicles, melt droplets, and melt

(See figure on next page.)

Fig. 5 Back-scattered electron images of major constituent phases in C0094, glossy group. **a** Euhedral hexagonal morphology of pyrrhotite and plaquette magnetite. Some pyrrhotites show smooth surface texture. **b** Pyrrhotite having modified surface. **c** Framboidal magnetite. **d** Cubic-shape magnetite. **e** Ca–Mg carbonate, dolomite. **f** Coarse-grained phyllosilicate. **g** Circular structure-enriched region. Larger ones are indicated by arrows. **h** High-resolution image of a circular structure. **i** Melt-droplet texture includes rounded opaque phases. **j** Melt-aggregate-like morphology showing tiny bubbles at the surface. **k** Line analysis profile of a circular structure obtained by EDS

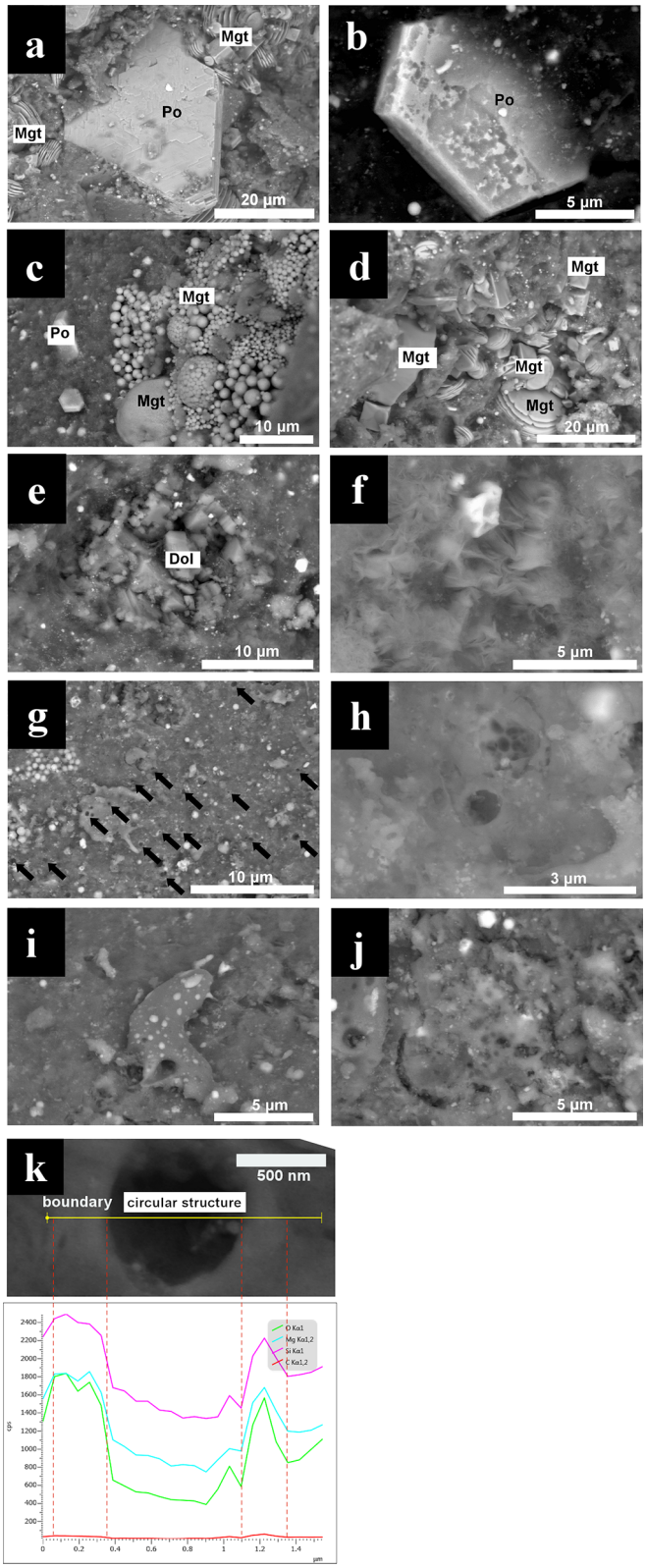

Fig. 5 (See legend on previous page.)

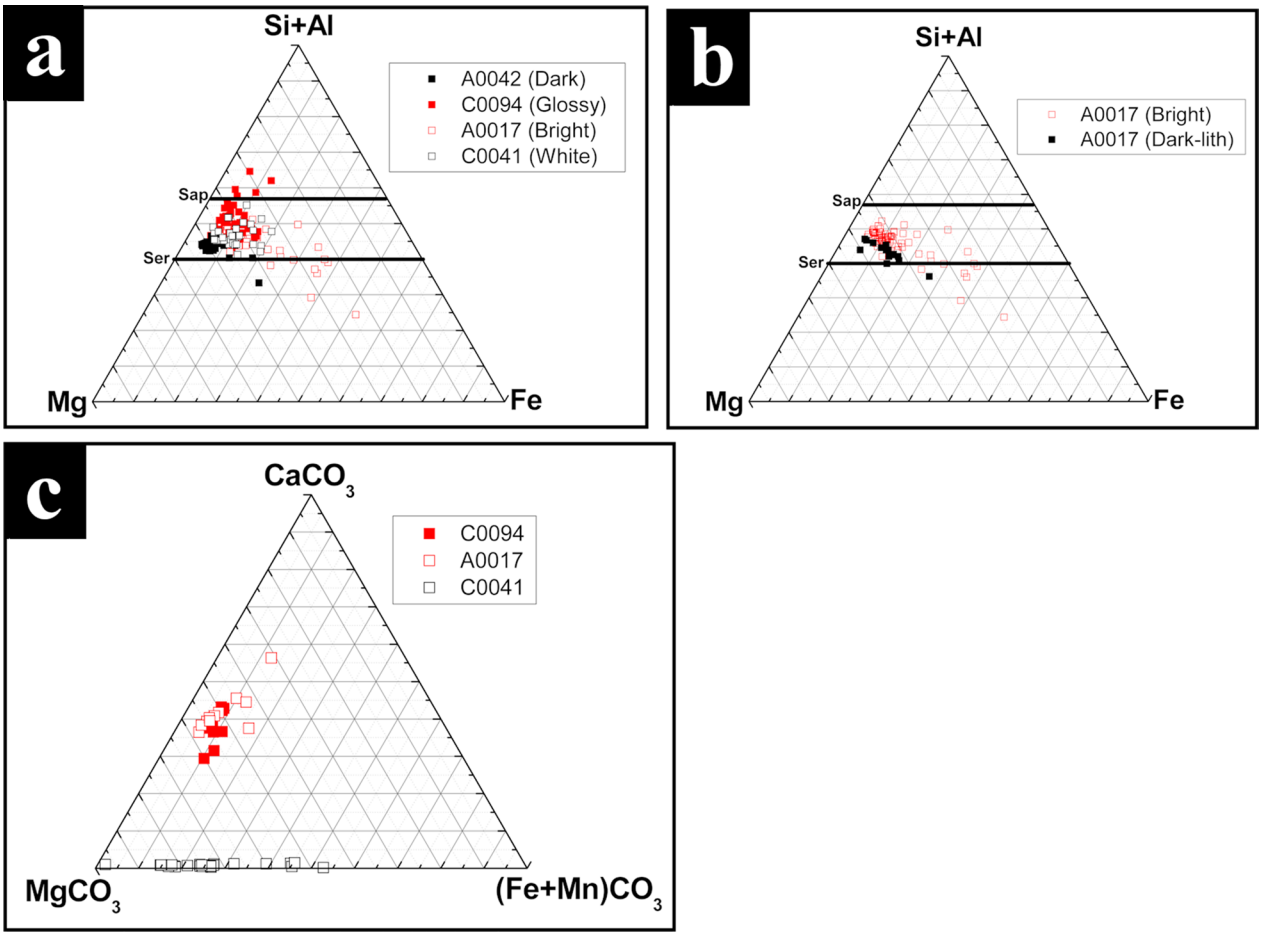

Fig. 6 Chemical compositions of matrices and carbonates. Ternary plots of matrices and carbonate compositions in four Ryugu grains obtained by EDS. **a** Matrix of each grain. All data plot in between smectite and serpentine compositions. **b** Bright and dark region of matrix in A0017. Although the bright area shows slightly higher content of Si, both plot within the compositional range of 4 grains shown in a. **c** Carbonate of each grain. Only C0041 contains Mg–Fe carbonates instead of dolomite

splashes. Given that the same features were observed on the back sides of the grains, we suggest that the grain orientation must have changed at least once, and possibly many times, since the asteroid formation. It is likely that shaking and gardening processes (Housen et al. 1979) caused the grains to roll over on the surface of Ryugu.

C0094 and A0017 were classified into the glossy and bright groups, respectively, and contain melt droplets with sizes of 5–20 μm. The melt droplets contain round opaque minerals. It is inferred that these droplets were once molten, rapidly cooled, and then solidified. In addition, there are some splash-like textures, such as melt threads emanating from the melt droplets. This indicates that the melt droplets were ejected in a molten state and then adhered to the grain surface. Melt aggregate layers were also observed in C0094 and A0017. The melt aggregate layer in C0094 is 5–10 μm in size and has a smooth structure. The layer observed on the back side of A0017

(See figure on next page.)

Fig. 7 Back-scattered electron images of major constituent phases in A0017, bright group. **a** Euhedral hexagonal morphology of pyrrhotite and plaquette magnetite. Some pyrrhotites show smooth surface texture. **b** Pyrrhotite having modified surface. The back side of A0017 only contains this modified pyrrhotite instead of smooth ones. **c** Framboidal and spherical magnetite. **d** Framboidal and plaquette shape magnetite. **e** Ca–Mg carbonate, dolomite. **f** Coarse-grained phyllosilicate. **g** Circular structure-enriched region. Larger ones are indicated by arrows. **h** High-resolution image of a circular structure. **i** Melt-droplet texture includes rounded opaque phases. **j** Melt-vein and –splash like morphologies. **k** Large melt-aggregate layer. **l** Enlarged view of a part of region shown in **j**. It has tiny bubbles and opaque minerals at the surface

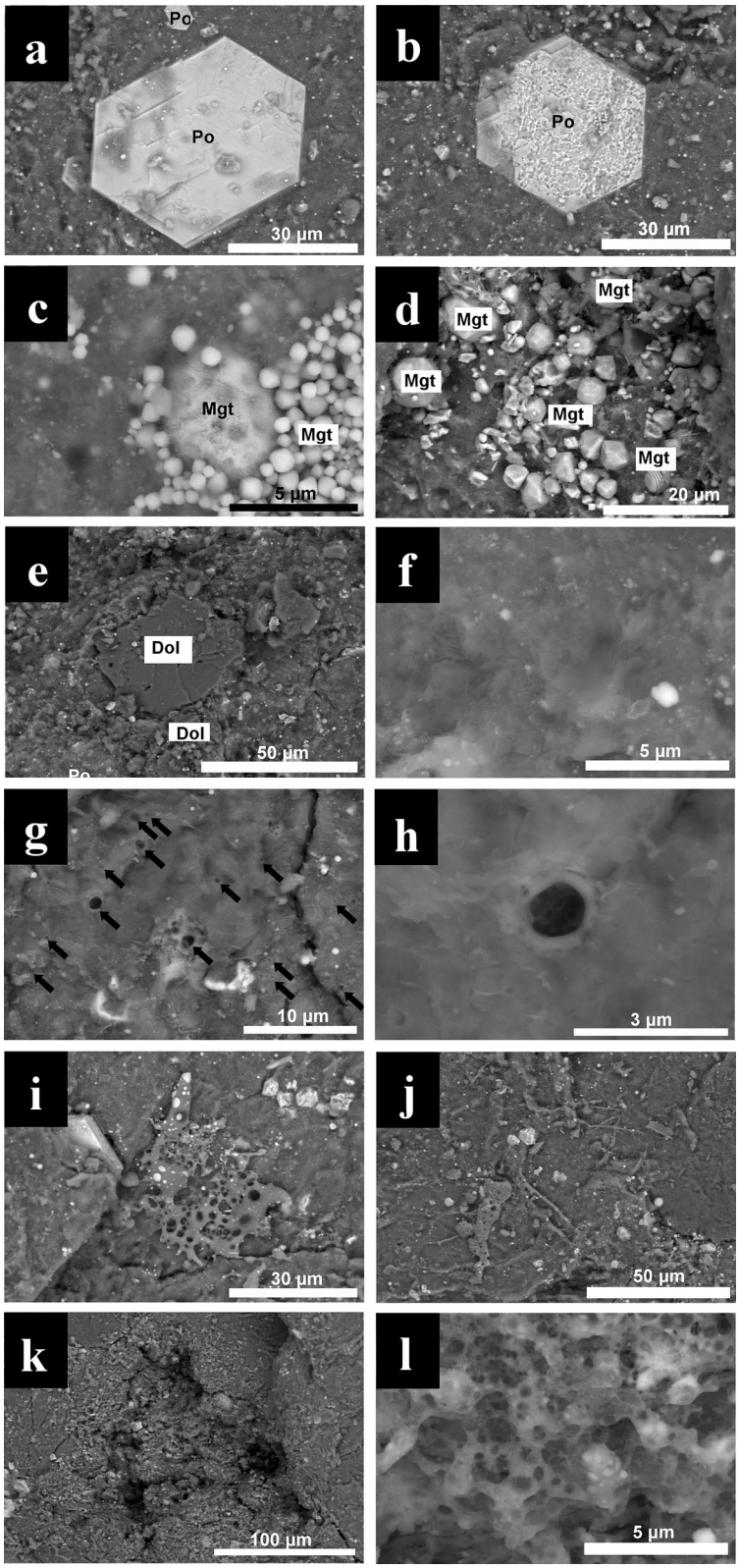

Fig. 7 (See legend on previous page.)

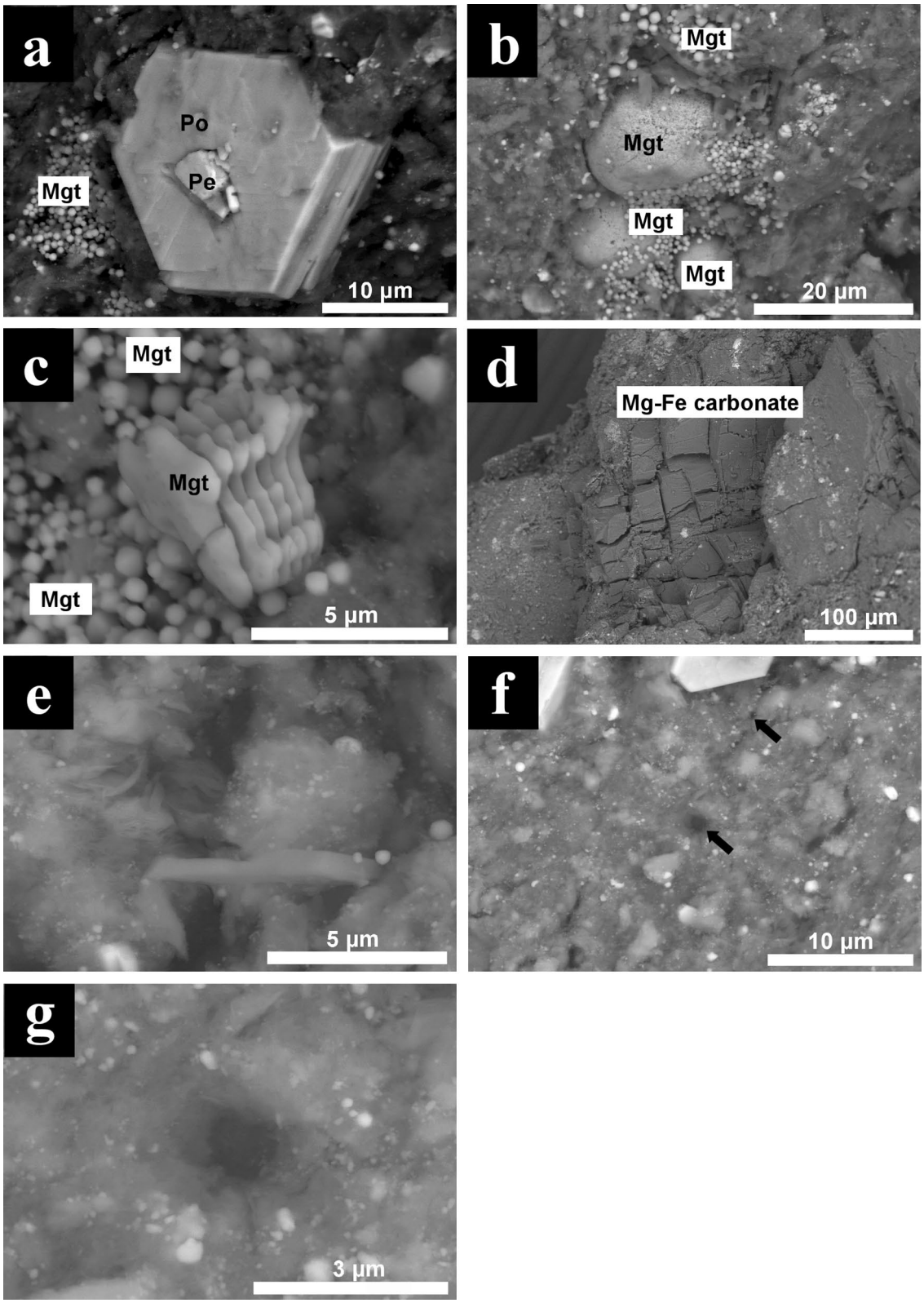

Fig. 8 Back-scattered electron images of major constituent phases in C0041, white group. **a** Euhedral hexagonal morphology of pyrrhotite showing a smooth texture. **b** Framboidal magnetite. **c** Plaquette magnetite. **d** Large Mg–Fe carbonate. **e** Coarse-grained phyllosilicate. **f** Circular structure-enriched region. Larger ones are indicated by arrows. **g** High-resolution image of a circular structure

covers ~ 200 μm^2, and rounded Fe sulfide grains were observed inside the void-rich structure. Melt aggregate layers have been recognized as one of the space weathering textures on small grains from Ryugu, based on detailed transmission electron microscopy (TEM)–EDS observations (Noguchi et al. 2022). Noguchi et al. propose a schematic accumulation history of space weathering on a Ryugu grain less than 100 μm in size based on the surface modification of phyllosilicate-rich matrix. As the first detectable space weathering effect on Ryugu grain, the smooth layer is formed on the phyllosilicate-rich matrix by the gradual accumulation of solar wind radiation damage. The smooth layer is completely amorphous, and the chemical composition is not able to distinguish from the surrounding phyllosilicate-rich matrix. For the next step, impact melt covers a grain partially to completely. The melt is identified as 'frothy layer' consisting of silicate glass embedded vesicles and submicroscopic rounded Fe–Ni sulfide beads. In this study, the texture in C0094 is consistent with that reported for the smooth layer, and that in A0017 is consistent with that reported for the frothy layer (Noguchi et al. 2022). The smooth layer was produced by solar wind irradiation, in which the crystal structure of layered silicate minerals is destroyed by solar wind implantation, which forms numerous bubbles on the surface layer. In contrast, the frothy layer is characterized by tiny opaque minerals, which are mostly sulfides and rare metallic Fe in the amorphous silicates, and formed by melting of the smooth layer. As such, the chemical composition of the bright lithology in A0017 has a wide range of Fe contents, which might reflect the presence of such a frothy layer. We would like to mention that even in A0017 and C0094, the detectable space weathering textures like smooth and frothy layers are observed only in part of the bright and glossy regions, without covering the entire region. In addition to the glossy and bright regions, melt splashes are also scattered across the grains.

On the back side of A0017, which includes frothy layer, only pyrrhotite with an altered surface was observed. The front surface of A0017 and both sides of C0094 have smooth layers, which coexist with altered and smooth pyrrhotite. Only smooth pyrrhotite were observed in A0042. Therefore, the pyrrhotite alteration may be a good proxy for estimating how long space weathering was experienced in the uppermost layer of the Ryugu parent body. Morphological alteration of space weathered pyrrhotite has been identified in Itokawa particles and lunar soils (Matsumoto et. al. 2020, 2021a). SEM observations of these returned samples revealed that iron sulfides have vesicular textures and iron whiskers on their surfaces. A similar altered pyrrhotite texture has been reported in previous studies of Ryugu grains (Matsumoto et al. 2021b; Noguchi et al. 2022). Matsumoto et al. (2021b) reported that the altered surfaces of pyrrhotite and pentlandite have vesicular rugged textures. They also found Fe whiskers protruding from sulfide grain surfaces. In this study, Fe whiskers have not been observed in any altered pyrrhotite. These burst vesicles on pyrrhotite were reproduced by pulse laser irradiation on Murchison CM2 meteorite to simulate micrometeoroid impact on airless body surfaces (Thompson et al. 2019; 2020). In contrast, even in the smooth surface of sulfides, the depletion of S and Ni due to solar wind irradiation was reported by previous studies Itokawa particles (Keller and Berger 2014; Chaves and Thompson 2022). Therefore, the pyrrhotite alteration may be a good indicator for space weathering but it is not perfectly applicable to the complex real-world space weathering process. However, it can be revealed that the altered sulfide experienced micrometeoroid impact regardless of whether they have undergone solar wind irradiation, we could suggest the frequency of the impacts, i.e., a part of the accumulation of space weathering on a scale that can be detected by SEM observations. This information is very useful, because even if TEM observation is not possible, quick SEM observation can be used to select samples with surfaces that have experienced space weathering due to micrometeorite impact. This study is the first to highlight how the degree of space weathering of individual returned grains could be determined from the JAXA curation database.

XRD data for A0042, which appears to be a typical and fresh rock fragment from Ryugu, were compared with the rock fragments (C0094 and A0017) exhibiting the space weathering textures, and no obvious difference was detected (Fig. 9). This may be because the target texture corresponding to the frothy layer in A0017 could not be separated out as an XRD sample. The frothy layer is located in depression on the grain surface and is surrounded by many radiating cracks. Therefore, we sampled avoiding the frothy layer, since it may have resulted in it being crushed. If the frothy layer is sampled properly using focused ion beam techniques, and XRD analysis is then undertaken, it is expected that tiny, low-crystallinity, Fe–Ni sulfide and amorphous silicates, as identified by TEM observations (Noguchi et al. 2022), would be detected. However, even in A0017, where the frothy layer covers a wide area of 200 μm^2, the altered region is only a small portion of the total surface area of A0017. In the case of millimeter-sized grains, it is expected that it will be difficult to identify the space weathering texture by XRD analysis of entire grains. Similarly, multiple 100-μm-sized XRD samples containing 5–10-μm-sized melt splashes have been analyzed, but the volume of the melt splashes with respect to the entire grain is too small to characterize them. The main minerals in the melt

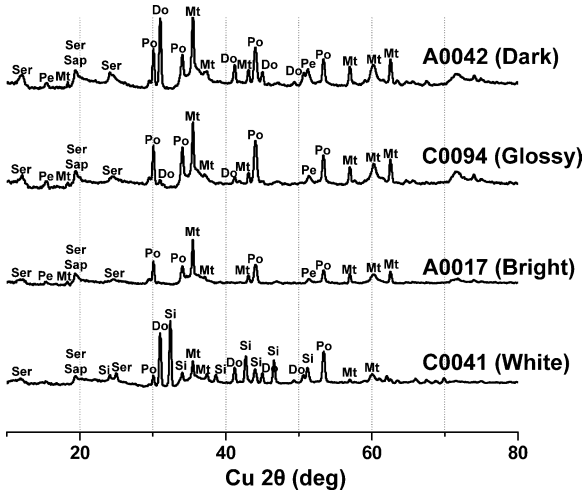

Fig. 9 Mineral combinations of each grain. Representative X-ray diffraction patterns obtained from 100 microns-sized fragment of each group. Each pattern was selected from the perspective that the most minerals are detected clearly. Ser: serpentine, Sap: saponite, Po: pyrrhotite, Pen: pentlandite, Mt: magnetite, Do: dolomite, Si: siderite. C0041 only shows sharp peaks of siderite

splashes are also amorphous silicate and tiny opaque minerals. As such, our XRD data cannot detect the presence or absence of melt splashes. Our results suggest that, although all four grains have experienced variable degrees of space weathering, it is difficult to determine the presence or absence of space weathered textures on individual grains by XRD for the following reasons. First, detectable space weathering textures (e.g., smooth and frothy layers), which are likely to be detectable by XRD, are localized on a grain and only represent a small proportion of the volume of an entire grain. Second, the main alteration process is the amorphization of phyllosilicates and formation of tiny sulfides, which is difficult to quantify from XRD patterns. The proportion of Ryugu grains having the space weathering features of A0017 (bright group) and C0094 (glossy group) is about 20% of the 205 grains (Table 1). Space weathered samples from the asteroid Itokawa and lunar regolith have an abundance of ~ 50%, which is clearly higher than for the Ryugu grains. This is also consistent with the large number of small grains from Ryugu (Noguchi et al. 2022). Although there is difficulty in comparing with Itokawa and lunar samples, because Ryugu samples have been possibly fragmented during the collection process, Ryugu samples should have more subsurface materials due to the successful injection of metal bullets during sample collection. Noguchi reported that only 3% and 10% in TD1 and TD2 sample of Ryugu, respectively, shows the severe surface modifications of the matrix. Our study shows that the proportion of Ryugu grains belonging to the bright group (e.g., A0017) that have experienced the longer accumulation of space weathering is about twice as high at TD1 site as compared with TD2 site (Table 1). This is because TD1 site is supposed to contain a higher proportion of surface material than TD2 site. The photographs taken before and after sampling by the onboard camera ONC-W1 of the Hayabusa2 spacecraft show that the subsurface materials may be darker than the materials on the uppermost surface layer (Morota et al. 2020). This supports the hypothesis that grains of the bright group correspond to the surface materials on Ryugu.

Comparison with spectral data in the curation catalog

The SEM and XRD results obtained in this study are summarized in Table 2.

In the dark group, pyrrhotite is only present as smooth (not altered). Most grains in this group are coated with fine powder. The glossy group contains both smooth and altered pyrrhotite. Melt droplets and smooth layers

Table 2 SEM observation and XRD results of JAXA-DD grains

Characteristic		Dark			Glossy		Bright		White
Sample ID		A0042	A0042 backside	C0041 backside	C0094	C0094 backside	A0017	A0017 backside	C0041
Pyrrhotite	smooth	○	○	○	○	○	○	○	○
	modified	–	–	–	○	○	○	○	–
Magnetite		○	○	○	○	○	○	○	○
Carbonate	dolomite	○	○	○	○	○	○	○	○
	Mg–Fe carbonate	–	–	–	–	–	–	–	○
Circular structures		○	○	○	○	○	○	○	○
Melt-droplet		–	–	–	○	○	○	○	–
Smooth layer		–	–	–	○	○	○	○	–
Frothy layer		–	–	–	–	–	○	○	–

○: detected, –: not detected

were found in this group. The bright group also contains smooth and altered pyrrhotite. On the back side of A0017 in the bright group, pyrrhotite occurs only as altered material and a texture similar to the frothy layer was observed. The grains in the bright group lack fine particles on their surfaces. The white group contains large Mg–Fe carbonate minerals. The distribution of this unique carbonate mineral coincides with white materials observed by optical microscopy. Based on these observational results, the spectroscopic data released in the curation database were carefully investigated.

The large Mg–Fe carbonate mineral in C0041 is evident in both the FTIR and MicrOmega spectra. A comparison with the spectroscopic data set, allows MicrOmega to determine that the mineral species is an (Fe, Mg)-carbonate (Loizeau et al. 2023).

The difference in the chemical composition of the carbonate minerals is considered to reflect compositional differences in the aqueous solutions during crystal growth. Given that the crystal size of the Mg–Fe carbonate mineral is larger than that of the dolomite (Yokoyama et al. 2022; Nakamura et al. 2022), and that the former is heterogeneously distributed in the Ryugu samples, not only the chemical composition of aqueous solutions but also the alteration process to form Mg–Fe carbonates might be different from the process that produced many small Ca–Mg carbonates. Although A0017 is a bright grain under an optical microscope, it is also a bright grain with high reflectance based on the MicrOmega spectrum, averaged over the surface of the grain. To compare the brightness of the 11 grains in the bright group and 15 grains in the dark group, reflectance at 2.0 and 3.0 μm corresponding to regions with no strong absorption features in the average spectral data from MicrOmega average spectra of each of these grains were obtained and plotted in Fig. 10. The average spectrum from MicrOmega for each grain is the average of all pixels corresponding to the grain excluding the boundary of surrounding a sapphire dish, the contribution from the signal reflected on the clean chamber window that is between MicrOmega and the sample is removed as much as possible (Riu et al., 2022; Yogata et al., in preparation). Figure 10 shows that the grains classified as bright under the optical microscope have an average reflectance that is ~ 20% brighter than the dark grains, even in the near-infrared region. However, the SEM observations showed that the entire area of A0017 is not covered with the frothy layer. It is necessary to verify with higher resolution techniques (e.g., TEM) what the brightness is related to. One possible factor is the presence of large saponite layer. Nakamura et al. (2022) reported that well-developed pure saponite layer makes the flat surface of the Ryugu grains. The flat surface reflects light well under an optical microscope and should appear brighter than the surrounding uneven surface. Another possibility is that the grain surfaces classified as being bright are not covered with fine particles. Since the surface of the dark grain consists of hydrous phyllosilicate matrix, the surface layer may have a larger amount of water and fine particles may tend to attach to the grain surface. On the other hand, a part of the phyllosilicate matrix on the surface of the bright grains could be dehydrated due to space weathering, which may make it difficult for the fine particles to adhere.

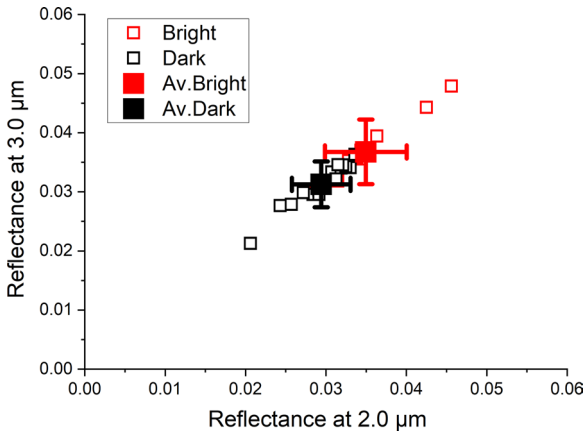

Fig. 10 Comparison of reflectance between bright and dark group. Reflectance at 2.0 and 3.0 μm of bright and dark group grains obtained by MicrOmega

Conclusions

A proposed morphological classification of grains from the asteroid Ryugu based on optical microscopy, and the data presented here, show that the classification reflects differences in the degree of space weathering and mineral assemblages. The grains of the dark group appear darker due to the effects of adhering tiny particles and surface irregularities, and have experienced little space weathering. Grains of the bright group appear relatively brighter and have few attached particles and irregularities. The bright group has experienced the most severe space weathering. The glossy group underwent a moderate degree of space weathering, and are shiny and dark under the optical microscope. The large white materials in the grains of the white group are an Mg–Fe carbonate mineral. This morphological classification is also consistent with the spectroscopic data published in the JAXA curation database. The Mg–Fe carbonate (or breunnerite) minerals were also detected by FTIR and MicrOmega, and the bright particles can be separated from the other three groups by their average reflectance obtained by MicrOmega.

The four morphological groups proposed in this study and the degree of space weathering indicate that the presence of altered pyrrhotite, smooth layer, and frothy layer are important proxies for space weathering. The degree of space weathering of the four studied grains is: weak = A0042 (dark group) and C0041 (white group); moderate = C0094 (glossy); severe = A0017 (bright). Compared with grains from Itokawa and the lunar regolith, few Ryugu samples have experienced severe space weathering, whereby entire millimeter-sized grains are altered. Severe space weathering may be indicated by the presence of altered pyrrhotite.

Although the four grains have a variety of appearances, the chemical composition and mineralogy of the matrix are similar to CI chondrites. No components other than those expected from parent bodies of carbonaceous chondrites such as exotic materials have yet been identified. As such, the Ryugu returned samples are relatively homogeneous and consist of carbonaceous chondrite material that has undergone aqueous alteration.

The results obtained in this study, along with the detailed results of the initial analysis team and Phase2 curation teams, will guide future researchers in the selection of samples to investigate from the curation database catalog.

Supplementary Information

The online version contains supplementary material available at https://doi.org/10.1186/s40623-022-01754-8.

Additional file 1. The classification table for all 205 grains. This is a summary of what morphological characteristics each grain has. If the characteristic is found, 1 is entered in the cell and the total number is calculated at the bottom of each column.

Acknowledgements
We greatly appreciate Prof. Takaaki Noguchi and Dr. Toru Matsumoto (Kyoto University) for helpful comments. We thank the whole Hayabusa2 team for the precious samples returned safely from Ryugu. We gratefully acknowledge support from the CNES (National Centre for Space Studies). We also thank all members of the Astromaterials Science Research Group (ASRG, JAXA), for discussions of the assessment procedure and facility management at the Extraterrestrial Samples Curation Center (ESCuC). Preliminary reports based on this paper were presented at Hayabusa 2021 (8th ISAS symposium of the Solar System Materials). Valuable comments and suggestions from Michelle S. Thompson and anonymous reviewer, which improved the manuscript significantly, and the editorial handling by Takeshi Sagiya and Kevin Righter are deeply appreciated.

Author contributions
AN led this work, conducted the assessment, analyzed and interpreted the data, and finalized the manuscript. TY, MN, KY, AM, KN, KH, KK, YH, and HS analyzed and interpreted the data about FTIR, MicrOmega, Microscopy, and Weighing obtained by curation initial description. JPB, CP, VH, RB, LR, LL, DL, TLPJ, and AMS analyzed, interpreted and constructed average spectra from MicrOmega data. TY, MA, TO, and TU supervised the assessment scheme and were major contributors in writing the manuscript. SN, TS, ST, FT, MY, SW, and YT led science operations of spacecraft. All authors read and approved the final manuscript.

Funding
Not applicable.

Availability of data and materials
The data sets analyzed during the current study are available in the Ryugu Sample Database System repository, [https://darts.isas.jaxa.jp/curation/hayabusa2/].

Declarations

Competing interests
The authors declare that they have no competing interests.

Author details
[1]Institute of Space and Astronautical Science (ISAS), Japan Aerospace Exploration Agency (JAXA), Sagamihara, Kanagawa 252-5210, Japan. [2]Institut d'Astrophysique Spatiale, UMR8617, CNRS/Université Paris-Saclay, 91405 Orsay, France. [3]ESAC, European Space Agency, Madrid, Spain. [4]Centre National d'Etudes Spatiales, 18 Avenue E. Belin, 31401 Toulouse, France. [5]Kanagawa Institute of Technology, Atsugi 243-0292, Japan. [6]Synchrotron Radiation Research Center, Nagoya University, Furo-cho, Chikusa-ku, Nagoya, Aichi 464-8603, Japan. [7]Marine Works Japan Ltd., 3-54-1 Oppama-higashi, Yokosuka 237-0063, Japan. [8]The Graduate University for Advanced Studies (SOKENDAI), Hayama 240-0193, Japan.

Received: 20 July 2022 Accepted: 14 December 2022
Published: 28 March 2023

References

Arakawa M, Saiki T, Wada K, Ogawa K, Kadono T, Shirai K, Sawada H, Ishibashi K, Honda R, Sakatani N, Iijima Y, Okamoto C, Yano H, Takagi Y, Hayakawa M, Michel P, Jutzi M, Shimaki Y, Kimura S, Mimasu Y, Toda T, Imamura H, Nakazawa S, Hayakawa H, Sugita S, Morota T, Kameda S, Tatsumi E, Cho Y, Yoshioka K, Yokota Y, Matsuoka M, Yamada M, Kouyama T, Honda C, Tsuda Y, Watanabe S, Yoshikawa M, Tanaka S, Terui F, Kikuchi S, Yamaguchi T, Ogawa N, Ono G, Yoshikawa K, Takahashi T, Takei Y, Fujii A, Takeuchi H, Yamamoto Y, Okada T, Hirose C, Hosoda S, Mori O, Shimada T, Soldini S, Tsukizaki R, Iwata T, Ozaki M, Abe M, Namiki N, Kitazato K, Tachibana S, Ikeda H, Hirata N, Hirata N, Noguchi R, Miura A (2020) An artificial impact on the asteroid (162173) Ryugu formed a crater in the gravity-dominated regime. Science 368:67–71. https://doi.org/10.1126/science.aaz1701

Chaves L, Thompson MS (2022) Space weathering signatures in sulfide and silicate minerals from asteroid Itokawa. Earth, Planets and Space 74:124. https://doi.org/10.1186/s40623-022-01683-6

Hatakeda K, Yada Y, Abe M, Okada T, Nakato A, Yogata K, Miyazaki A, Kumagai K, Nishimura M, Hitomi Y, Soejima H, Nagashima K, Yoshitake M, Iwamae A, Furuya S, Usui T, Tachibana S, Sakamoto K, Kitazono K, Yurimoto H (2023) Homogeneity and heterogeneity in Near-Infrared FTIR spectra of Ryugu returned samples. Earth, Planets and Space. https://doi.org/10.1186/s40623-023-01784-w

Housen KR, Wilkening LL, Chapman CR, Greenberg R (1979) Asteroidal regoliths. Icarus 39:317–351. https://doi.org/10.1016/0019-1035(79)90145-3

Ito M, Tomioka N, Uesugi K, Uesugi M, Kodama Y, Sakurai I, Okada I, Ohigashi T, Yuzawa H, Yamaguchi A (2020) The universal sample holders of micro-analytical instruments of FIB, TEM, NanoSIMS, and STXM-NEXAFS for the coordinated analysis of extraterrestrial materials. Earth, Planets and Space 72:133. https://doi.org/10.1186/s40623-020-01267-2

Jaumann R, Schmitz N, Ho T-M, Schröder SE, Otto KA, Stephan K, Elgner S, Krohn K, Preusker F, Scholten F, Biele J, Ulamec S, Krause C, Sugita S, Matz K-D, Roatsch T, Parekh R, Mottola S, Grott M, Michel P, Trauthan F, Koncz A, Michaelis H, Lange C, Grundmann JT, Maibaum M, Sasaki K, Wolff F, Reill J,

Moussi-Soffys A, Lorda L, Neumann W, Vincent J-B, Wagner R, Bibring J-P, Kameda S, Yano H, Watanabe S, Yoshikawa M, Tsuda Y, Okada T, Yoshimitsu T, Mimasu Y, Saiki T, Yabuta H, Rauer H, Honda R, Morota T, Yokota Y, Kouyama T (2019) Images from the surface of asteroid Ryugu show rocks similar to carbonaceous chondrite meteorites. Science 365:817–820. https://doi.org/10.1126/science.aaw8627

Keller LP, Berger E (2014) A transmission electron microscope study of Itokawa regolith grains. Earth, Planets and Space 66:71. https://doi.org/10.1186/1880-5981-66-71

Loizeau D, Pilorget C, Riu L, Brunetto R, Bibring JP, Nakato A, Aléon-Toppani A, Hatakeda K, Yogata K, Carter J, Le Pivert-Jolivet T, Yada T, Okada T, Usui T, Langevin Y, Lantz C, Baklouti D, Miyazaki A, Nishimura M, Nagashima K, Kumagai K, Hitomi Y, Abe M, Saiki T, Tanaka S, Nakazawa S, Tsuda Y, Watanabe S (2023) Constraints on solar system early evolution by MicrOmega analysis of Ryugu carbonates. Nat Astron 12:1

Matsumoto T, Hasegawa S, Nakao S, Sakai S, Yurimoto H (2018) Population characteristics of submicrometer-sized craters on regolith particles from asteroid Itokawa. Icarus 303:22–33. https://doi.org/10.1016/j.icarus.2017.12.017

Matsumoto T, Harries D, Langenhorst F, Miyake A, Noguchi T (2020) Iron whiskers on asteroid Itokawa indicate sulfide destruction by space weathering. Nat Commun 11:1117. https://doi.org/10.1038/s41467-020-14758-3

Matsumoto T, Noguchi T, Tobimatsu Y, Harries D, Langenhorst F, Miyake A, Hidaka H (2021a) Space weathering destruction by space weathering. Geochim Cosmochim Acta 299:69–84. https://doi.org/10.1016/j.gca.2021.02.013

Matsumoto T, Noguchi T, Miyake A, Igami Y, Haruta M, Saito H, Hata S, Seto Y, Miyahara M, Tomioka T, Ishii HA, Bradley JP, Ohtaki K, Dobrică E, Nakamura T, Matsumoto M, Tsuchiyama A, Yasutake M, Matsuno J, Okumura S, Uesugi K, Uesugi M, Takeuchi A, Sun M, Enju S, Takigawa A, Leroux H, Le Guillou C, Jacob D, Marinova M, de la Peña F, Langenhorst F, Harries D, Beck P, Van Phan TH, Rebois R, Abreu NM, Zega T, Zanetta PM, Thompson M, Lee M, Daly L, Bland P, Stroud R, Burgess K, Bridges JC, Hicks L, Zolensky ME, Frank DR, Martinez J, Yurimoto H, Nagashima K, Kawasaki K, Okazaki R, Yabuta H, Naraoka H, Sakamoto K, Tachibana S, Watanabe S, Tsuda Y, and the Hayabusa2 Initial Analysis Team (2021b) Surface morphologies and space weathering features of Ryugu samples. In: Abstracts of the 8th Hayabusa Symposium, ISAS/JAXA, Sagamihara. 17–18. https://curation.isas.jaxa.jp/symposium/abstract/2021/Abstracts_day1.pdf

Morota T, Sugita S, Cho Y, Kanamaru M, Tatsumi E, Sakatani N, Honda R, Hirata N, Kikuchi H, Yamada M, Yokota Y, Kameda S, Matsuoka M, Sawada H, Honda C, Kouyama T, Ogawa K, Suzuki H, Yoshioka K, Hayakawa M, Hirata N, Hirabayashi M, Miyamoto H, Michikami T, Hiroi T, Hemmi R, Barnouin OS, Ernst CM, Kitazato K, Nakamura T, Riu L, Senshu H, Kobayashi H, Sasaki S, Komatsu G, Tanabe N, Fujii Y, Irie T, Suemitsu M, Takaki N, Sugimoto C, Yumoto K, Ishida M, Kato H, Moroi K, Domingue D, Michel P, Pilorget C, Iwata T, Abe M, Ohtake M, Nakauchi Y, Tsumura K, Yabuta H, Ishihara Y, Noguchi R, Matsumoto K, Miura A, Namiki N, Tachibana S, Arakawa M, Ikeda H, Wada K, Mizuno T, Hirose C, Hosoda S, Mori O, Shimada T, Soldini S, Tsukizaki R, Yano H, Ozaki M, Takeuchi H, Yamamoto Y, Okada T, Shimaki Y, Shirai K, Iijima Y, Noda H, Kikuchi S, Yamaguchi T, Ogawa N, Ono G, Mimasu Y, Yoshikawa K, Takahashi T, Takei Y, Fujii A, Nakazawa S, Terui F, Tanaka S, Yoshikawa M, Saiki T, Watanabe S, Tsuda Y (2020) Sample collection from asteroid (162173) Ryugu by Hayabusa 2: implications for surface evolution. Science 368:654–659. https://doi.org/10.1126/science.aaz6306

Nakamura T, Matsumoto M, Amano K, Enokido Y, Zolensky M, Mikouchi T, Genda H, Tanaka S, Zolotov M, Kurosawa K, Wakita S, Hyoudo R, Nagano H, Nakashima D, Takahashi Y, Fujioka Y, Kikuiri M, Kagawa E, Matsuoka M, Brealey A, Tsuchiyama A, Uesugi M, Matsuno J, Kimura Y, Sato M, Milliken M, Tatsumi E, Sugita S, Hiroi T, Kitazono K, Brownlee D, Joswiak D, Takahashi M, Ninomiya K, Osawa T, Terada K, Brenker F, Tkalcec B, Vincze L, Brunetto R, Aleon-Toppani A, Chan Q, Roskosz M, Vinnet J, Beck P, Alp E, Michikami T, Nagaashi Y, Tsuji T, Ino Y, Martinez J, Han J, Dolocan H, Bodnar R, Tanaka M, Yoshida H, Sugiyama K, King A, Fukushi K, Suga H, Yamashita S, Kawai T, Inoue K, Nakato A, Noguchi T, Vilas F, Hendrix A, Jaramillo C, Lorin D, Dominguez G, Gainsforth Z, Engrand C, Duprat J, Russell S, Bonato E, Ma C, Kawamoto T, Wada T, Watanabe S, Endo R, Enju S, Riu L, Rubino S, Tack P, Takeshita S, Takeichi Y, Takeuchi A, Takigawa A, Takir D, Tanigaki T, Taniguchi A, Tsukamoto K, Yagi T, Yamada S, Yamamoto K, Yamashita Y, Yasutake M, Uesugi K, Umegaki K, I-Huan C, Ishizaki Y, Okumura S, Palomba E, Pilorget C, Potin S, Abdulkareem A, Anada S, Araki Y, Sakatani N, Schulz C, Sekizawa O, Sitzman S, Sugiura K, Sun M, Dartois E, De Pauw E, Dionnet Z, Djouadi Z, Falkenberg G, Fujita R, Fukuma T, Gearba I, Hagiya K, Hu M, Kato T, Kawamura T, Kimura M, Kubo M, Langenhorst F, Lantz C, Lavina B, Lindner M, Vekemans B, Baklouti D, Bazi B, Borondics F, Nagasawa S, Nishiyama G, Nitta K, Mathurin J, Matsumoto T, Mitsukawa I, Miura H, Miyake A, Miyake Y, Yurimoto H, Okazaki R, Yabuta H, Naraoka H, Sakamoto K, Tachibana S, Connolly Jr D, Lauretta D, Yoshitake M, Yoshikawa M, Yoshihara K, Yokota Y, Yogata K, Yano H, Yamamoto Y, Yamamoto D, Yamada M, Yada T, Wada K, Usui T, Tsukizaki R, Terui F, Takeuchi H, Takei Y, Suzuki A, Soejima H, Shirai K, Shimaki Y, Senshu H, Sawada H, Saiki T, Ozaki M, Ono G, Okadda T, Ogawa N, Ogawa K, Noguchi R, Noda H, Nishimura M, Namiki N, Nakazawa S, Morota T, Miyazaki A, Miura A, Mimatsu Y, Matsumoto K, Kumagai K, Kouyama T, Kikuchi S, Kawahara K, Kameda S, Iwata T, Ishihara Y, Ishiguro M, Ikeda H, Hosoda S, Honda R, Honda C, Hitomi Y, Hirata N, Hirata N, Hayakawa M, Hatakeda K, Furuya S, Fukai R, Fujii A, Cho Y, Arakawa M, Abe M, Watanabe S, Tsuda Y (2022) Formation and evolution of carbonaceous asteroid Ryugu: Direct evidence from returned samples. Science, eabn8671. https://doi.org/10.1126/science.abn8671

Noguchi T, Matsumoto T, Miyake A, Igami Y, Haruta M, Saito H, Hata S, Seto Y, iyahara M, Tomioka N, Ishii HA, Bradley JP, Ohtaki K, Dobrică E, Leroux H, Le Guillou C, Jacob D, de la Peña F, Laforet S, Marinova M, Langenhorst F, Harries D, Beck P, Phan THV, Rebois R, Abreu NM, Gray J, Zega T, Zanetta PM, Thompson MS, Stroud R, Burgess K, Cymes BA, Bridges JC, Hicks L, Lee MR, Daly L, Bland PA, Zolensky ME, Frank DR, Martinez J, Tsuchiyama A, Yasutake M, Matsuno J, Okumura S, Mitsukawa I, Uesugi K, Uesugi M, Takeuchi A, Sun M, Enju S, Takigawa A, Michikami T, Nakamura T, Matsumoto M, Nakauchi Y, Abe M, Arakawa M, Fujii A, Hayakawa M, Hirata N, Hirata N, Honda R, Honda C, Hosoda S, Iijima Y, Ikeda H, Ishiguro M, Ishihara Y, Iwata T, Kawahara K, Kikuchi S, Kitazato K, Matsumoto K, Matsuoka M, Mimasu Y, Miura A, Morota T, Nakazawa S, Namiki N, Noda H, Noguchi R, Ogawa N, Ogawa K, Okada T, Okamoto C, Ono G, Ozaki M, Saiki T, Sakatani N, Sawada H, Senshu H, Shimaki Y, Shirai K, Sugita S, Takei Y, Takeuchi H, Tanaka S, Tatsumi E, Terui F, Tsukizaki R, Wada K, Yamada M, Yamada T, Yamamoto Y, Yano H, Yokota Y, Yoshihara K, Yoshikawa M, Yoshikawa K, Fukai R, Furuya S, Hatakeda K, Hayashi T, Hitomi Y, Kumagai K, Miyazaki A, Nakato A, Nishimura M, Soejima H, Suzuki AI, Usui T, Yada T, Yamamoto D, Yogata K, Yoshitake M, Connolly, Jr. HC, Lauretta DS, Yurimoto H, Nagashima K, Kawasaki N, Sakamoto N, Okazaki R, Yabuta H, Naraoka H, Sakamoto K, Tachibana S, Watanabe S, Tsuda Y (2022) A dehydrated space weathered skin cloaking the hydrated interior of Ryugu. Nature. Accepted.

Pilorget C, Okada T, Hamm V, Brunetto R, Yada T, Loizeau D, Riu L, Usui T, Moussi-Soffys A, Hatakeda K, Nakato A, Yogata K, Abe M, Aléon-Toppani A, Carter J, Chaigneau M, Crane B, Gondet B, Kumagai K, Langevin Y, Lantz C, Le Pivert-Jolivet T, Lequertier G, Lourit L, Miyazaki A, Nishimura M, Poulet F, Arakawa M, Hirata N, Kitazato K, Nakazawa S, Namiki N, Saiki T, Sugita S, Tachibana S, Tanaka S, Yoshikawa M, Tsuda Y, Watanabe S, Bibring JP (2021a) First compositional analysis of Ryugu samples by the MicrOmega hyperspectral microscope. Nat Astron 6:221–225. https://doi.org/10.1038/s41550-021-01549-z

Pilorget C, Fernando J, Riu L, Kitazato K, Iwata T (2021b) Global-scale albedo and spectro-photometric properties of Ryugu from NIRS3/Hayabusa2, implications for the composition of Ryugu and the representativity of the returned samples. Icarus 355:114126. https://doi.org/10.1016/j.icarus.2020.114126

Riu L, Pilorget C, Hamm V, Bibring JP, Lantz C, Loizeau D, Brunetto R, Carter J, Lequetier G, Lourit L, Okada T, Yogata K, Hatakeda K, Nakato A, Yada T (2022) Calibration and performances of MicrOmega instrument for the characterization of asteroid Ryugu returned samples. Rev Sci Instrum 93:054503. https://doi.org/10.1063/5.0082456

Sawada H, Okazaki R, Tachibana S, Sakamoto K, Takano Y, Okamoto C, Yano H, Miura Y, Abe M, Hasegawa S, Noguchi T, Hayabusa2 Sampler Team (2017) Hayabusa2 sampler: collection of asteroidal surface material. Space Sci Rev 208:81–106. https://doi.org/10.1007/s11214-017-0338-8

Tachibana S, Sawada H, Okazaki R, Takano Y, Sakamoto K, Miura YN, Okamoto C, Yano H, Yamanouchi S, Michel P, Zhang Y, Schwartz S, Thuillet F, Yurimoto H, Nakamura T, Noguchi T, Yabuta H, Naraoka H, Tsuchiyama A, Imae N, Kurosawa K, Nakamura AM, Ogawa K, Sugita S, Morota T, Honda R, Kameda S, Tatsumi E, Cho Y, Yoshioka K, Yokota Y, Hayakawa

M, Matsuoka M, Sakatani N, Yamada M, Kouyama T, Suzuki H, Honda C, Yoshimitsu T, Kubota T, Demura H, Yada T, Nishimura M, Yogata K, Nakato A, Yoshitake M, Suzuki AI, Furuya S, Hatakeda K, Miyazaki A, Kumagai K, Okada T, Abe M, Usui T, Ireland TR, Fujimoto M, Yamada T, Arakawa M, Connolly HC Jr, Fujii A, Hasegawa S, Hirata N, Hirata N, Hirose C, Hosoda S, Iijima Y, Ikeda H, Ishiguro M, Ishihara Y, Iwata T, Kikuchi S, Kitazato K, Lauretta DS, Libourel G, Marty B, Matsumoto K, Michikami T, Mimasu Y, Miura A, Mori O, Nakamura-Messenger K, Namiki N, Nguyen AN, Nittler LR, Noda H, Noguchi R, Ogawa N, Ono G, Ozaki M, Senshu H, Shimada T, Shimaki T, Shirai K, Soldini S, Takahashi T, Takei Y, Takeuchi H, Tsukizaki R, Wada K, Yamamoto Y, Yoshikawa K, Yumoto K, Zolensky ME, Nakazawa S, Terui F, Tanaka S, Saiki T, Yoshikawa M, Watanabe S, Tsuda Y (2022) Pebbles and sands on asteroid (162173) Ryugu: on-site observation and returned particles from two landing sites. Science 375:1011–1016. https://doi.org/10.1126/science.abj8624

Tatsumi E, Domingue D, Yokota Y, Schroder S, Hasegawa S, Kuroda D, Ishiguro M, Hiroi T, Honda R, Hemmi R, Le Corre L, Sakatani N, Morota T, Yamada M, Kameda S, Koyama T, Suzuki H, Cho Y, Yoshioka K, Matsuoka M, Honda C, Hayakawa M, Hirata N, Hirata N, Yamamoto Y, Vilas F, Takato N, Yoshikawa M, Abe M, Sugita S (2020) Global photometric properties of (162173) Ryugu. Astron Astrophys 639:A83. https://doi.org/10.1051/0004-6361/201937096

Thompson MS, Loeffler MJ, Morris RV, Keller LP, Christoffersen R (2019) Spectral and chemical effects of simulated space weathering of the Murchison CM2 carbonaceous chondrite. Icarus 319:499–511. https://doi.org/10.1016/j.icarus.2018.09.022

Thompson MS, Morris RV, Clemett SJ, Loeffler MJ, Trang D, Keller LP, Christoffersen R, Agresti DG (2020) The efect of progressive space weathering on the organic and inorganic components of a carbonacous chondrite. Icarus 346:113775. https://doi.org/10.1016/j.icarus.2020.113775

Tsuda Y, Saiki T, Terui F, Nakazawa S, Yoshikawa M, Watanabe S, Hayabusa2 Project Team (2020) Hayabusa2 mission status: Landing, roving and cratering on asteroid Ryugu. Acta Astronaut 171:42–54. https://doi.org/10.1016/j.actaastro.2020.02.035

Yada T, Abe M, Okada T, Nakato A, Yogata K, Miyazaki A, Hatakeda K, Kumagai K, Nishimura M, Hitomi Y, Soejima H, Yoshitake M, Iwamae A, Furuya S, Uesugi M, Karouji Y, Usui T, Hayashi T, Yamamoto D, Fukai R, Sugita S, Cho Y, Yumoto K, Yabe Y, Bibring J-P, Pilorget C, Hamm V, Brunetto R, Riu L, Lourit L, Loizeau D, Lequertier G, Moussi-Soffys A, Tachibana S, Sawada H, Okazaki R, Takano Y, Sakamoto K, Miura YN, Yano H, Ireland TR, Yamada T, Fujimoto M, Kitazato K, Namiki N, Arakawa M, Hirata N, Yurimoto H, Nakamura T, Noguchi T, Yabuta H, Naraoka H, Ito M, Nakamura E, Uesugi K, Kobayashi K, Michikami T, Kikuchi H, Hirata N, Ishihara Y, Matsumoto K, Noda H, Noguchi R, Shimaki Y, Shirai K, Ogawa K, Wada K, Senshu H, Yamamoto Y, Morota T, Honda R, Honda C, Yokota Y, Matsuoka M, Sakatani N, Tatsumi E, Miura A, Yamada M, Fujii A, Hirose C, Hosoda S, Ikeda H, Iwata T, Kikuchi S, Mimasu Y, Mori O, Ogawa N, Ono G, Shimada T, Soldini S, Takahashi T, Takei Y, Takeuchi H, Tsukizaki R, Yoshikawa K, Terui F, Nakazawa S, Tanaka S, Saiki T, Yoshikawa M, Watanabe S-I, Tsuda Y (2022) Preliminary analysis of the Hayabusa2 samples returned from C-type asteroid Ryugu. Nat Astron 6:214–220. https://doi.org/10.1038/s41550-021-01550-6

Yamaguchi A (2020) Curation of antarctic meteorites in national institute of polar research. Polar News 56:23–29

Yokoyama T, Nagashima K, Nakai I, Young ED, Abe Y, Aléon J, Alexander CMO'D, Amari S, Amelin Y, Bajo K, Bizzarro M, Bouvier A, Carlson RW, Chaussidon M, Choi B, Dauphas N, Davis AM, Di Rocco T, Fujiya W, Fukai R, Gautam I, Haba MK, Hibiya Y, Hidaka H, Homma H, Hoppe P, Huss GR, Ichida K, Iizuka T, Ireland TR, Ishikawa A, Ito M, Itoh S, Kawasaki N, Kita NT, Kitajima K, Kleine T, Komatani S, Krot AN, Liu M, Masuda Y, McKeegan KD, Morita M, Motomura K, Moynier F, Nguyen A, Nittler L, Onose M, Pack A, Park C, Piani L, Qin L, Russel SS, Sakamoto N, Schönbächler M, Tafla L, Tang H, Terada K, Terada Y, Usui T, Wada S, Wadhwa M, Walker RJ, Yamashita K, Yin Q, Yoneda S, Yui H, Zhang A, Connolly HC Jr, Lauretta DS, Nakamura T, Naraoka H, Noguchi T, Okazaki R, Sakamoto K, Yabuta H, Abe M, Arakawa M, Fujii A, Hayakawa M, Hirata N, Honda R, Honda C, Hosoda S, Iijima Y, Ikeda H, Ishiguro M, Ishihara Y, Iwata T, Kawahara K, Kikuchi S, Kitazato K, Matsumoto K, Matsuoka M, Michikami T, Mimasu Y, Miura A, Morota T, Nakazawa S, Namiki N, Noda H, Noguchi R, Ogawa N, Ogawa K, Okada T, Okamoto C, Ono G, Ozaki M, Saiki T, Sakatani N, Sawada H, Senshu H, Shimaki Y, Shirai K, Sugita S, TakeiY, Takeuchi H, Tanaka S, Tatsumi E, Terui F, Tsuda Y, Tsukizaki R, Wada K, Watanabe S, Yamada M, Yamada T, Ymamoto Y, Yano H, Yokota Y, Yoshihara K, Yoshikawa M, Yoshikawa K, Furuya S, Hatakeda K, Hayashi T, Hitomi Y, Kumagai K, Miyazaki A, Nakato A, Nishimura M, Soejima H, Suzuki A, Yada T, Yamamoto D, Yogata K, Yoshitake M, Tachibana S, Yurimoto H (2022) Samples returned from the asterioid Ryugu are similar to Ivuna-type carbonaceous meteorites. Science. https://doi.org/10.1126/science.abn7850

Publisher's Note